

Defects and oxidation resilience in InSe

K.J. Xiao* and A. Carvalho†

*Centre for Advanced 2D Materials and Graphene Research Centre,
National University of Singapore, Singapore 117542, Singapore*

A. H. Castro Neto

*Centre for Advanced 2D Materials and Graphene Research Centre,
National University of Singapore, Singapore 117542, Singapore and
Boston University, 590 Commonwealth Avenue, Boston, Massachusetts 02215, USA*

(Dated: October 16, 2018)

We use density functional theory to study intrinsic defects and oxygen related defects in indium selenide. We find that InSe is prone to oxidation, but however not reacting with oxygen as strongly as phosphorene. The dominant intrinsic defects in In-rich material are the In interstitial, a shallow donor, and the Se vacancy, which introduces deep traps. The latter can be passivated by oxygen, which is isoelectronic with Se. The dominant intrinsic defects in Se-rich material have comparatively higher formation energies.

I. INTRODUCTION

Amongst two-dimensional materials, the families of chalcogenides such as transition metal dichalcogenides, group-III and IV monochalcogenides often offer the advantages of stability and the possibility of fabrication by epitaxial growth methods that can be scaled up—such as vapor transport epitaxy of chemical vapor deposition (CVD),¹ and chemical vapor transport.² Indium selenide,³ which shares the same crystal structure with GaS and InS,⁴ has recently been mechanically exfoliated into few layer flakes.^{5–7} Thin InSe flakes have been used for phase change memory devices and image sensing,^{8–10} and has been suggested to be a functional material for water splitting.¹¹ With respect to the electronic properties, few layer InSe has been shown to have an extraordinary electron mobility exceeding 10^3 and $10^4 \text{ cm}^{-2}/(\text{Vs})$ at room and liquid-helium temperatures, in few layers, making it one of the highest known mobility 2D materials.^{7,12} This is consistent with the bulk electron mobility, which is also the highest amongst isomorphic group-III chalcogenides, according to Hall effect measurements.¹³ Even though it is often n -type, InSe can also be p -type and in that case it can be interesting for different purposes: It has a very high effective mass for holes near the Γ point, where there is a ‘Mexican-hat’-type van-Hove singularity.^{4,14–16} Such a singularity gives rise to a ferromagnetic instability at low temperatures.¹⁷ Different from other materials with ‘Mexican-hat’-type bands such as SnO, the singularity is present in the valence band both for monolayer and for few-layer material.¹⁶

Thus, since both p - and n -type conduction regimes are of technological interest, it is desirable to be able to effectively control the type and amount of defects and impurities unintentionally introduced. Sn and Pb, when present, can act respectively as a shallow donor and shallow acceptor. The first is often cited as the origin of the p -type conductivity. However, intrinsic shallow donors that cannot be ascribed to any impurity and disappear upon

annealing have been found as well.^{13,18,19} These were speculated to be related to Se deficiency.¹⁹ According to previous theoretical calculations, adsorbed or interstitial In has low formation energy in In-rich material,¹⁰ parallel to what has been found for the Ga interstitial in GaS,²⁰ However, many studies of point defects in III-VI materials have been restricted to vacancies or substitutional type defects.^{10,11,21–24} Thus, specific defect signatures of the intrinsic shallow donors have not been assigned yet.

Interstitial atoms are supposed to increase the mechanical hardness of bulk GaSe by coupling the planar layers,^{25,26} and the same has been found for other ionized dopants as well.²⁷

In addition to intrinsic defects, it is important to investigate the defects caused by the interaction with oxygen and other atmospheric contaminants. The recently achieved high mobility transistor devices were fabricated with BN-encapsulated InSe layers, that were thus prevented from contact with the atmosphere.⁷ Still, InSe seems to be relatively stable in contact with air, as cleaved bulk surfaces show no signs of degradation at room temperature,^{28,29} comparing e.g. with phosphorene.

In this article, we will provide a detailed theoretical account of the properties of intrinsic defects and oxygen-related defects in InSe. In addition, we will discuss their impact on the electronic properties of the material, in particular discussing the identity of the shallow donors in unintentionally doped InSe.

II. METHODS

Parameters

The first principles calculations were performed by the density functional theory (DFT)^{30,31} implementation known as QUANTUM ESPRESSO.^{32,33} All of the computations were done consistently using the following parameters. The pseudopotentials used were given

by the projector augmented wave (PAW)^{34,35} approximation, and the exchange-correlation functional chosen was the generalized gradient approximation parametrized by Perdew, Burke, and Ernzerhof (GGA-PBE).³⁶ Specifically, the Pseudopotential Library (PSL)^{37,38} were used. A plane wave basis with kinetic energy cutoff of 42 Ry was used, and the k -point samples in the Brillouin zone were calculated with the Γ -centered $4 \times 4 \times 1$ Monkhorst-Pack³⁹ grid unless otherwise specified. Defect ionization transition levels were calculated with a k -point grid of $8 \times 8 \times 1$ centered upon Γ , with relaxation. All transition levels presented were at most 0.02 eV from their values when calculated with the smaller k -point grid. All geometries were relaxed to at least the default convergence thresholds (Forces $< 10^{-3}$ a.u.). The vacuum spacing along the z -axis was six times the lattice parameter of the primitive cell of the pristine monolayer, to avoid spurious interactions. All supercells consisted of 3×3 primitive unit cells.

Finally, to find the migration activation energies for the relevant defects, we also performed nudged elastic band calculations, without climbing images nor spins.

Formation Energies & Transition Levels

The formation energy of defect D is given by

$$E_f(D) = E(D) - \sum_i n_i \mu_i \quad (1)$$

where $E(D)$ is the energy of the supercell containing the defect, and n_i and μ_i are the number of atoms of species i and its chemical potential, respectively. The chemical potentials were evaluated both in the In-rich and Se-rich limit. In the In-rich case, the In potential was obtained from the elemental material in the α -In, tetragonal form. The Se chemical potential $\mu_{\text{Se, In-rich}}$ in the In-rich regime was obtained from the constraint

$$E(\text{PS}) = \sum_j n_j \mu_{j, \text{In-rich}} \quad (2)$$

where PS is the pristine supercell. A similar definition was used to obtain the chemical potentials in the Se-rich limit for which we used the trigonal $hP3$ Se allotrope as reference. The chemical potential for oxygen is obtained from molecular oxygen.

The defect ionization transition levels $E_D(q/q+1)$, defined by the Fermi level at which the formation energy of the defects in charge state q is the same as in charge state $q+1$, were found using the marker method, which is more accurate for 2D systems due to the cancellation of systematic errors⁴⁰. The ionization potential I_D and electron affinity A_D are defined by

$$I_D = E(D^+) - E(D^0), \quad A_D = E(D^0) - E(D^-). \quad (3)$$

The transition levels for acceptors $E_D(-/0)$ (donors $E_D(0/+)$) relative to valence band maximum E_v (downwards from conduction band minimum E_c), are given by

$$E_D(-/0) - E_v = E_g - [E_c - E_D(-/0)] = E_g - [A_D - A_{PS}] \quad (4a)$$

$$E_c - E_D(0/+) = E_g - [E_D(0/+) - E_v] = E_g - [I_{PS} - I_D] \quad (4b)$$

III. RESULTS

A. Intrinsic Point Defects

This work considered seven intrinsic point defects (Fig. 1): the indium vacancy (V_{In}), the anti-site defect consisting of a selenium replacing for indium (Se_{In}), indium replacing for selenium (In_{Se}), a swapped In-Se next-neighbor pair ($\text{In}_{\text{Se}}\text{-Se}_{\text{In}}$), that we will name “swap”, the selenium vacancy V_{Se} , selenium interstitial at the hexagonal interstitial site (In_{ic}), and above the center of the hexagonal interstitial cage (In_{ac}).

The respective band structures are represented in Fig. 2. The indium vacancy is a shallow acceptor (Fig. 2a). Se_{In} has a similar band structure, but the states originating in the In vacancy are half-filled and move towards mid-gap, whereas the conduction band is little perturbed (Fig. 2b). The other anti-site defect also has semi-filled states, whereas the combined swap of neighboring In and Se results in filled defect states near the valence band (Fig. 2c,d). The selenium vacancy introduces defect states both near the valence and conduction band (Fig. 2e). Finally, the indium interstitials are shallow donors (Fig. 2f,g). The In_{ac} configuration, the most stable (about 1.59 eV lower in energy than the In_{ic} configuration), changes little the conduction band dispersion, however donates free holes to the conduction band states.

The formation energies as a function of the Se chemical potential over all available range are shown in Fig. 3. As expected, in the In-rich regime the dominant defects are the Se vacancy and the In interstitial, whereas in the Se-rich limit the dominant defects are the In vacancy and the anti-site where Se replaces In. These regimes will be considered in more detail in the next sections.

1. In-rich regime

InSe crystals are typically grown using the Bridgmann method, from non-stoichiometric melts with In excess, resulting in In-rich crystals.^{13,18,19} This is expected due to the higher volatility of Se compared to In.

In this regime, the most stable defect, of the four defects we have considered, is an In interstitial above the hexagonal cage, closely followed by the Se vacancy, the latter of which seems to make a triangular bond between the three In atoms surrounding the vacancy. Both are donors (Fig. 2), with transition levels at 2.17 eV and 0.4 eV above the valence band, respectively (Table I). In

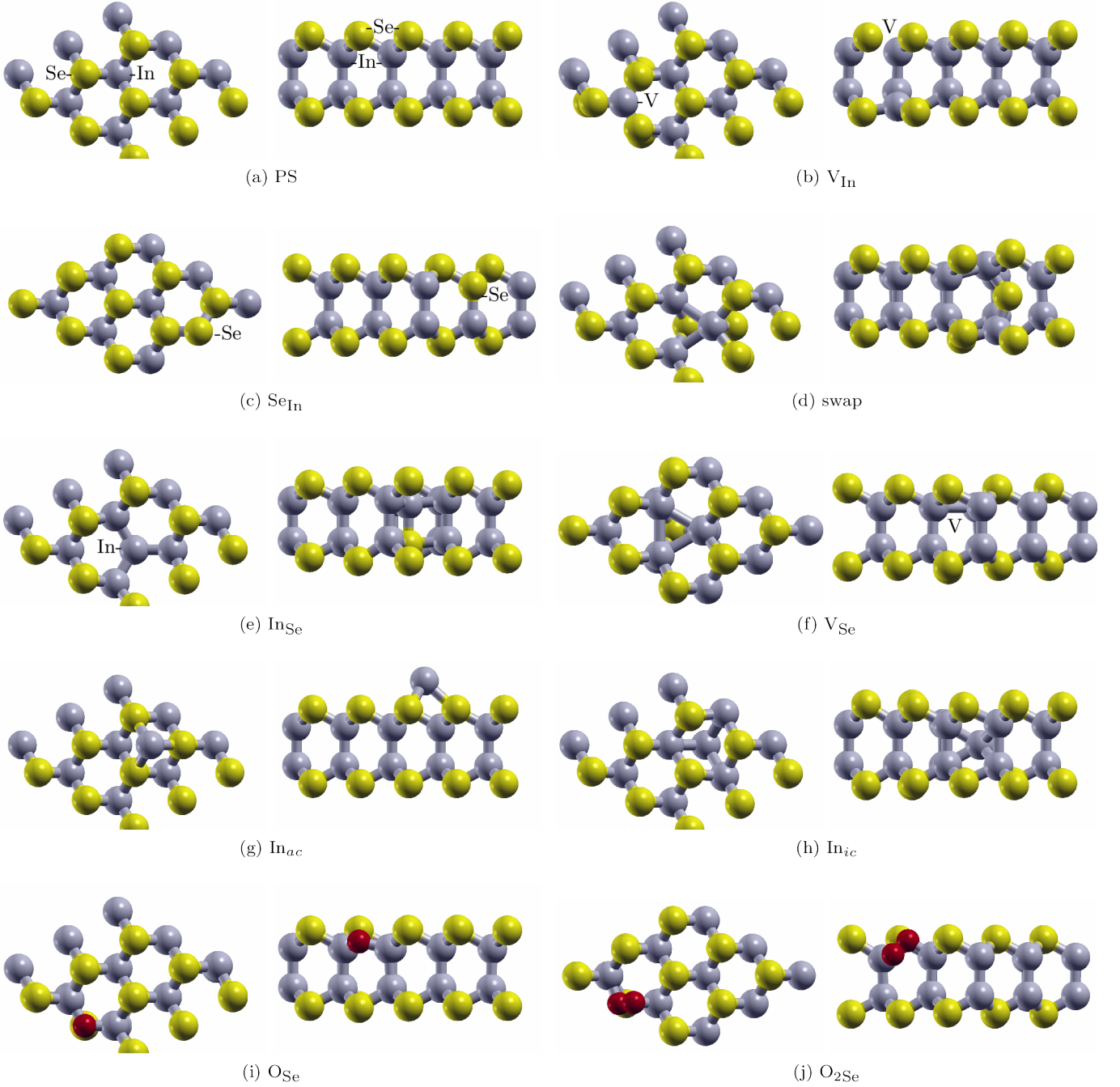


FIG. 1. (Color online) Top (0001) and side (1120) views of various intrinsic point defects and substitutional oxygen in monolayer InSe, grouped by similarity. (a) PS: pristine supercell. (b) V_{In} : indium vacancy. (c) Se_{In} : selenium-in-indium anti-site. (d) swap: swapping adjacent selenium and indium. (e) In_{Se} : indium-in-selenium anti-site. (f) V_{Se} : selenium vacancy. (g) In_{ac} : indium hovering above the center of the hexagonal interstitial cage. (h) In_{ic} : interstitial indium at center of hexagonal cage. (i) O_{Se} : oxygen atom substituting a selenium. (j) $\text{O}_{2\text{Se}}$: oxygen molecule substituting a selenium.

particular, the In interstitial, being a shallow donor, is likely to be the source of the n -type conduction in this material, as previously suggested following Hall effect measurements and position lifetime experiments^{18,19,43}. Experimentally, the defect ionization energy is 18 meV, consistent with the calculations, that effectively place

the transition level close to the conduction band bottom, within the method accuracy.⁴³ Furthermore, the experimentally observed donor center concentration is known to increase upon annealing at 470 K and the donor defects do not affect the positron lifetime, showing that it is an intrinsic defect and unlikely to be of vacancy type.⁴³

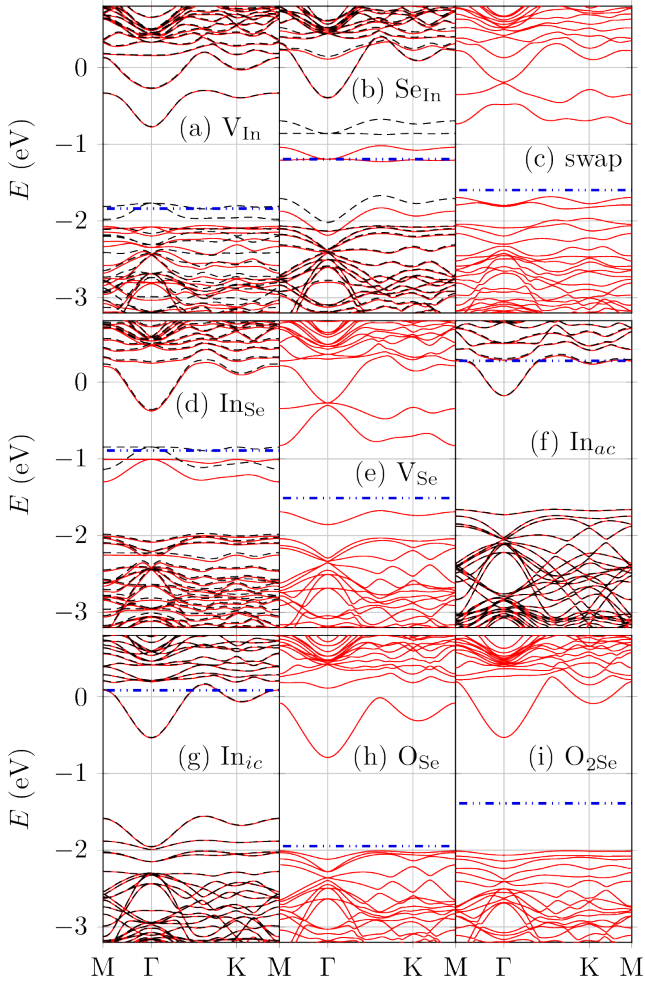


FIG. 2. (Color online) DFT band structure plots of various intrinsic point defects and substitutional oxygen defects in monolayer InSe: (a) V_{In} : indium vacancy. (b) Se_{In} : selenium-in-indium anti-site. (c) swap: swapping adjacent selenium and indium. (d) In_{Se} : indium-in-selenium anti-site. (e) V_{Se} : selenium vacancy. (f) In_{ac} : indium hovering above the center of the hexagonal interstitial cage. (g) In_{ic} : interstitial indium at center of hexagonal cage. (h) O_{Se} : oxygen atom substituting a selenium. (i) $\text{O}_{2\text{Se}}$: oxygen molecule substituting a selenium. Refer to Fig. 1 for the respective defects. Majority and minority spin bands are represented by continuous and dashed lines, respectively. Fermi levels are represented by blue dash-dotted horizontal lines.

TABLE I. Ionization potential and electron affinity *differences* of the various defects in monolayer InSe, which can be subtracted from $E_g(\approx 2.4\text{ eV})$ ^{3,10,41,42} to provide the activation energies via marker method (see text). All energies are in eV.

Defect	$E_D(0/+) - E_v$	$E_c - E_D(-/0)$
In_{ac}	2.17	
V_{Se}	0.40	0.65
Se_{In}	0.97	1.22
V_{In}		1.60
$\text{O}_2\text{-A}$		0.16

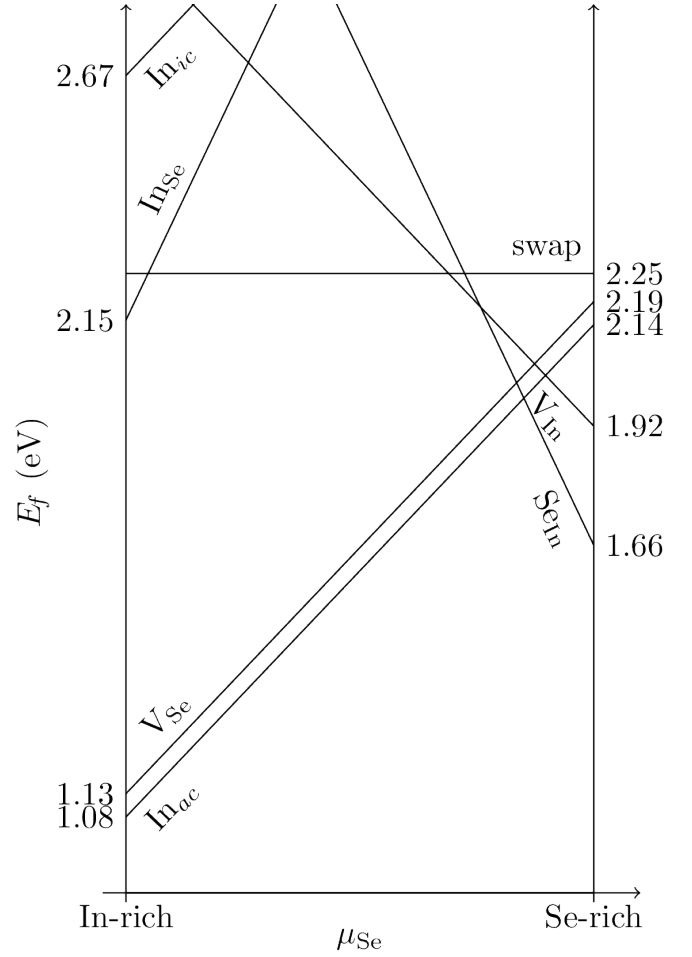


FIG. 3. Formation Energies E_f as a function of chemical potential μ_{Se} (arbitrary units) for intrinsic defects. $\Delta\mu_{\text{Se}} = 1.05\text{ eV}$. Refer to text for constraints and definitions.

Focusing on the annealing, we performed a nudged elastic band calculation for both the indium interstitial and the selenium vacancy in the monolayer case, obtaining migration activation energies of about 0.21 eV for In_{ac} and 1.5 eV for V_{Se} , in agreement with expectations. In addition, we note that the anti-site is energetically expensive, such that it should be rare, and does not contribute to doping. These establish that the In interstitial is responsible for the n -type character of undoped samples.

2. Se-rich regime

The two relevant intrinsic defects in this regime are the In vacancy and Se-replacing-In anti-site. V_{In} is a shallow acceptor, with transition levels calculated to lie 1.60 eV below the conduction band (Table I). However, since In is placed in the inside of the layer, it is unlikely that V_{In} would exist on its own, without the removal of neighboring Se as well. Se_{In} is both a donor and an acceptor, with possibly a negative- U level ordering (Table I).

TABLE II. Formation energies for each of the various stable oxygen absorption defects in monolayer InSe. Refer to Fig. 4 and Fig. 6 for meaning of abbreviated names. All energies are in eV.

Defect	E_f	Defect	E_f
O ₂ -A	-0.02	O-A	-1.65
O ₂ -B	-0.02	O-B	-1.64
O ₂ -C	-0.01	O-C	0.05
O ₂ -D	-0.01	O-D	0.37
O ₂ -E	-0.00	O-E	0.74
O ₂ -F	-0.00	O-F	1.07
O ₂ -G	0.95	O-G	2.61
(a) Physisorbed oxygen molecules.		(b) Chemisorbed oxygen atoms.	

B. O₂ Physisorption

Figure 4 shows the top and side views of all the possible configurations for oxygen molecule physisorption onto InSe. The formation energies are nearly the same (within 10 meV) for all the configurations A-F (Table IIa). The respective band structures, shown in Fig. 5, are also nearly identical, having no gap states for the majority spin and a double-degenerate empty gap state for minority spin. The coloring of the band structure plot helps reveal the deeply embedded impurity states beneath the valence band, which are flat, similar to the degenerate impurity gap states (dashed lines) in the band gap. The last of the structures considered, O₂-G, consists of an oxygen molecule inside the interstitial cage. This is 0.97 eV higher in energy than surface physisorbed molecules (Table IIa). Physisorbed oxygen can therefore in principle act as electron acceptor, as found in graphene,⁴⁴ phosphorene⁴⁵, and transition metal dichalcogenides⁴⁶

C. O Chemisorption

Chemisorption requires breaking the O₂ bond, which is found to have an energy of 6.61 eV in our calculations, a typical overestimation, on the high side, under the PBE approximation⁴⁷ (experimentally measured to be 5.12 eV⁴⁷). Nevertheless, we found that the chemisorption of oxygen is energetically favorable compared to physisorption.

Figure 6 shows the top and side views of all the single oxygen atom addition defects, while the band structure plots are presented in Fig. 7. The formation energies E_f do not depend on the In and Se chemical potentials (Table IIb).

Table IIb shows that there is a pair of essentially degenerate defects that are the lowest in energy. They are the O-A configuration, interstitial oxygen defect between two indium atoms, near the bond-center, venturing out into the hexagonal interstitial cage, and the O-B configuration, interstitial oxygen also near the bond-center

between two indium atoms, but underneath the indium-selenium bond. The other defects are considerably higher in energy. The band structure plots then tell us that the three defects of this class, the lowest in energy, are basically of the same type, and that they barely differ from the band structure of the PS.

Since chemisorbed oxygen defects have no levels in the gap, their interaction with vacancies to form substitutional defects will not be of the Coulomb type but possible strain mediated, since interstitial atoms, contrary to vacancies, introduce compressing strain on the surrounding lattice. In the next section, we will consider the defects resulting of the interaction between chemisorbed oxygen and selenium vacancies.

D. O Substitution Defects

We have considered the possibility that a Se lattice site is occupied by an oxygen atom or by an oxygen molecule (Fig. 1i,j). The respective band structures are shown in Fig. 2h,i. The formation energies of these defects are negative for all the range of chemical potentials, but are lowest in In-rich conditions (Fig. 8). They seem to neither be donors nor acceptors, just passivating the *p*-type selenium vacancy and reducing the band gap energy. The single substitutional oxygen atom is 0.87 eV lower in energy than the substitutional oxygen molecule, and it is the most energetically favorable defect presented in this paper. It is especially likely to form in the presence of chalcogen vacancies,⁴⁸ through the reaction



which has an enthalpy balance of 3.10 eV per oxygen atom.

IV. CONCLUSION

We have investigated the fundamental intrinsic defects in InSe, finding that in Se-rich material the Se_{In} anti-site is the dominant effect, whereas in In-rich material the indium interstitial and selenium vacancy are the dominant defects. Our calculations suggest that the unintentional *n*-type doping in cleanly-grown InSe should be due to the indium interstitial, which is a shallow donor, in agreement with arguments from experiments.

Selenium vacancies have donor deep states at about 0.4 eV above the valence band, that can partially compensate the doping by interstitials, but this state can be removed by reaction with molecular oxygen to form substitutional oxygen at the Se site, which has a positive energy balance of 3.10 eV.

In the absence of intrinsic defects, oxygen chemisorption and substitution is still energetically favorable, with such defects having formation energies E_f between -0.9

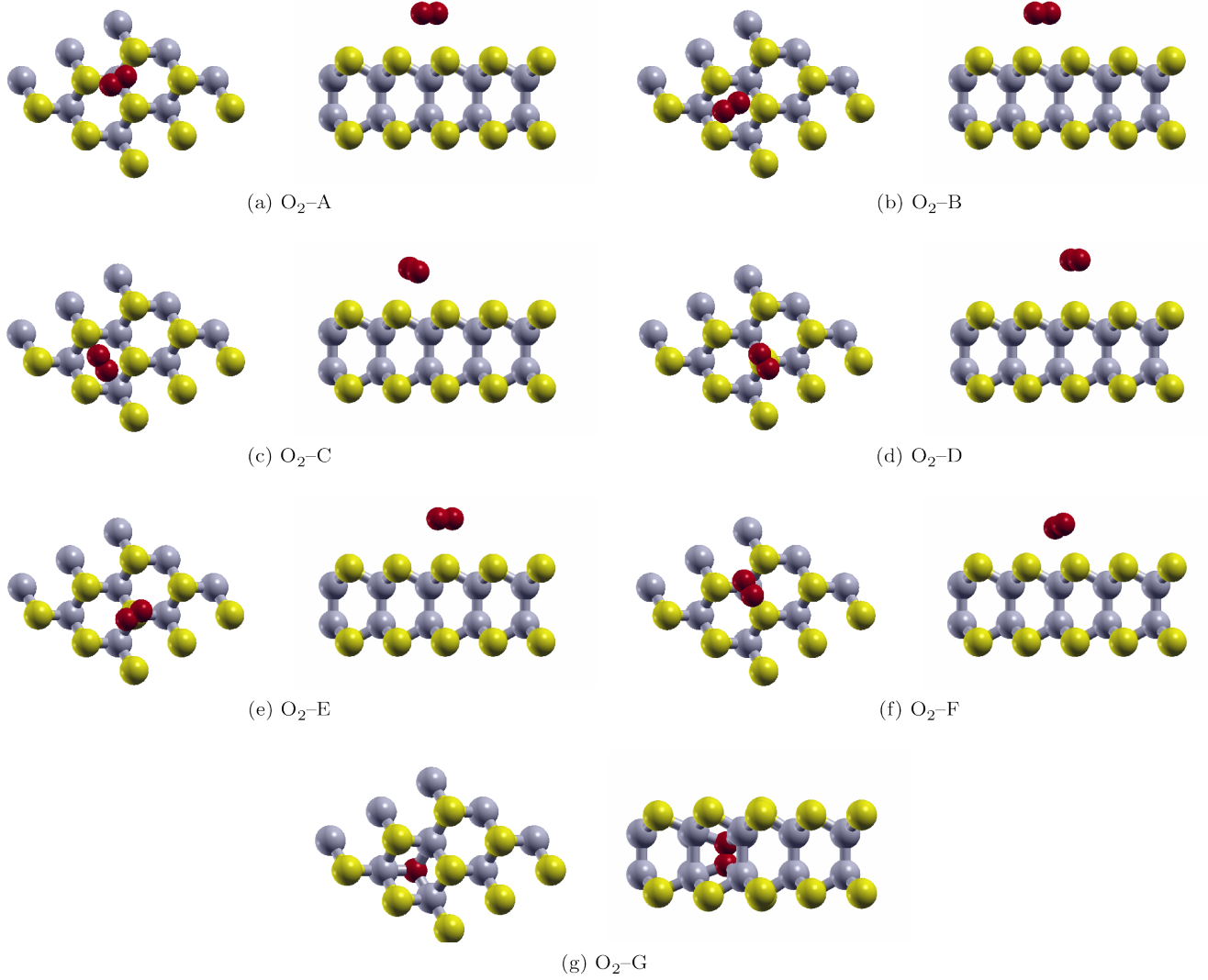


FIG. 4. (Color online) Top (0001) and side ($11\bar{2}0$) views of the stable single oxygen molecule addition defects in monolayer InSe (physisorption), in increasing order of relative energy cost of formation. (a) O_2 -A: above indium, perpendicular to bridge bond. (b) O_2 -B: above center of hexagonal cage, perpendicular to bridge bonds. (c) O_2 -C: above center of hexagonal cage, along bridge bonds. (d) O_2 -D: above selenium, along bridge bond. (e) O_2 -E: above selenium, perpendicular to bridge bond. (f) O_2 -F: above indium, along bridge bond. (g) O_2 -G: interstitial molecule at center of hexagonal cage, perpendicular to monolayer.

and -2 eV. Thus, InSe monolayers are prone to oxidation, but still considerably stronger in resilience against the chemisorption of oxygen than that in phosphorene (the respective enthalpies for oxygen chemisorption are -1.65 eV in InSe and -2.08 eV in phosphorene⁴⁹).

We find that chemisorbed oxygen and substitutional oxygen do not have, in their most stable forms, any ionization levels in the gap. However, since chemisorbed oxygen atoms are most stable inside the layer and between In sub-layers, the structural distortion and perturbation of the charge density distribution induced by

chemisorbed oxygen defects may reduce the carrier mobility, justifying the use of encapsulating layers in InSe-based electronic devices.

ACKNOWLEDGEMENTS

This work was supported by the National Research Foundation, Prime Minister Office, Singapore, under its Medium Sized Centre Programme and CRP award “Novel 2D materials with tailored properties: beyond graphene” (Grant number R-144-000-295-281). The first-principles calculations were carried out on the CA2DM high-performance computing facilities.

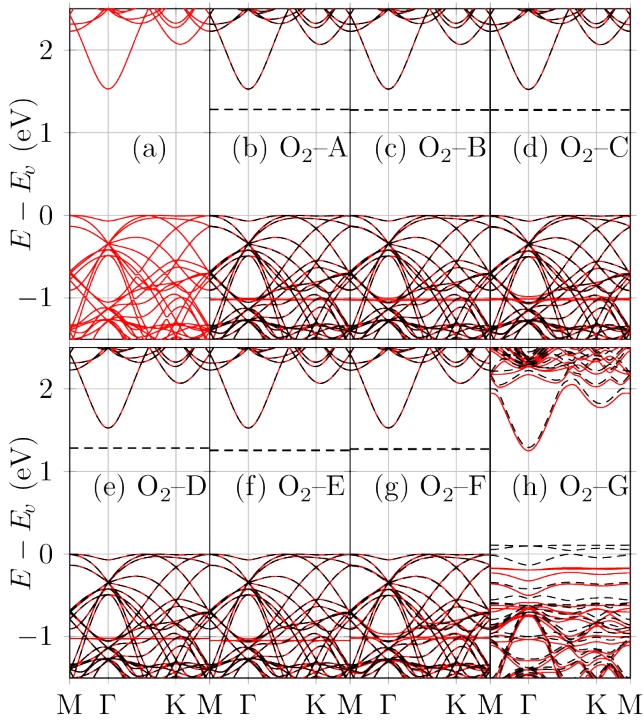


FIG. 5. (Color online) DFT band structure plots of various stable single oxygen molecule defects in monolayer InSe (Physisorption) in increasing order of relative energy cost of formation. (a) Pristine 3x3 supercell; (b)–(h) different configurations of oxygen defects. Refer to Fig. 4 for the respective defects. Minority spin is shown in dashed line. Color makes deeply embedded impurity states easier to see.

* c2dxk@nus.edu.sg

† carvalho@nus.edu.sg

¹ J. Yu, J. Li, W. Zhang, and H. Chang, *Chem. Sci.* **6**, 6705 (2015).

² C.-H. Ho, *2D Mat.* **3**, 025019 (2016).

³ J. F. Sánchez-Royo, G. Muñoz-Matutano, M. Brotons-Gisbert, J. P. Martínez-Pastor, A. Segura, A. Cantarero, R. Mata, J. Canet-Ferrer, G. Tobias, E. Canadell, J. Marqués-Hueso, and B. D. Gerardot, *Nano Res.* **7**, 1556 (2014).

⁴ V. Zólyomi, N. D. Drummond, and V. I. Fal'ko, *Phys. Rev. B* **89**, 205416 (2014).

⁵ S. Deckoff-Jones, J. Zhang, C. E. Petoukhoff, M. K. L. Man, S. Lei, R. Vajtai, P. M. Ajayan, D. Talbayev, J. Madéo, and K. M. Dani, *Sci. Rep.*, 22620 (2016).

⁶ G. W. Mudd, S. A. Svatek, T. Ren, A. Patan, O. Makarovskiy, L. Eaves, P. H. Beton, Z. D. Kovalyuk, G. V. Lashkarev, Z. R. Kudrynskiy, and A. I. Dmitriev, *Adv. Mat.* **25**, 5714 (2013).

⁷ D. A. Bandurin, A. V. Tyurnina, G. L. Yu, A. Mishchenko, V. Zólyomi, S. V. Morozov, R. K. Kumar, R. V. Gorbachev, Z. R. Kudrynskiy, S. Pezzini, Z. D. Kovalyuk, U. Zeitler, K. S. Novoselov, A. Patanè, L. Eaves, I. V. Grigorieva, V. I. Fal'ko, A. K. Geim, and Y. Cao, *Nat Nano advance online publication* (2016).

⁸ S. Lei, F. Wen, B. Li, Q. Wang, Y. Huang, Y. Gong, Y. He, P. Dong, J. Bellah, A. George, L. Ge, J. Lou, N. J. Halas, R. Vajtai, and P. M. Ajayan, *Nano Lett.* **15**, 259 (2015), pMID: 25517502.

⁹ G. A. Gibson, A. Chaiken, K. Nauka, C. C. Yang, R. Davidson, A. Holden, R. Bicknell, B. S. Yeh, J. Chen, H. Liao, S. Subramanian, D. Schut, J. Jasinski, and Z. Liliental-Weber, *Appl. Phys. Lett.* **86**, 051902 (2005).

¹⁰ Y. Guo and J. Robertson, arXiv preprint (2017).

¹¹ Q. Peng, R. Xiong, B. Sa, J. Zhou, C. Wen, B. Wu, M. Anpo, and Z. Sun, *Catal. Sci. Technol.* **7**, 2744 (2017).

¹² C. Sun, H. Xiang, B. Xu, Y. Xia, J. Yin, and Z. Liu, *Appl. Phys. Express* **9**, 035203 (2016).

¹³ A. Segura, F. Pomer, A. Cantarero, W. Krause, and A. Chevy, *Phys. Rev. B* **29**, 5708 (1984).

¹⁴ S. J. Magorrian, V. Zólyomi, and V. I. Fal'ko, *Phys. Rev. B* **94**, 245431 (2016).

¹⁵ D. V. Rybkovskiy, A. V. Osadchy, and E. D. Obraztsova, *Phys. Rev. B* **90**, 235302 (2014).

¹⁶ G. W. Mudd, M. R. Molas, X. Chen, V. Zólyomi, K. Nogajewski, Z. R. Kudrynskiy, Z. D. Kovalyuk, G. Yusa, O. Makarovskiy, L. Eaves, M. Potemski, V. I. Fal'ko, and A. Patanè, *Sci. Rep.* **6**, 39619 (2016).

¹⁷ L. Seixas, A. S. Rodin, A. Carvalho, and A. H. Castro Neto, *Phys. Rev. Lett.* **116**, 206803 (2016).

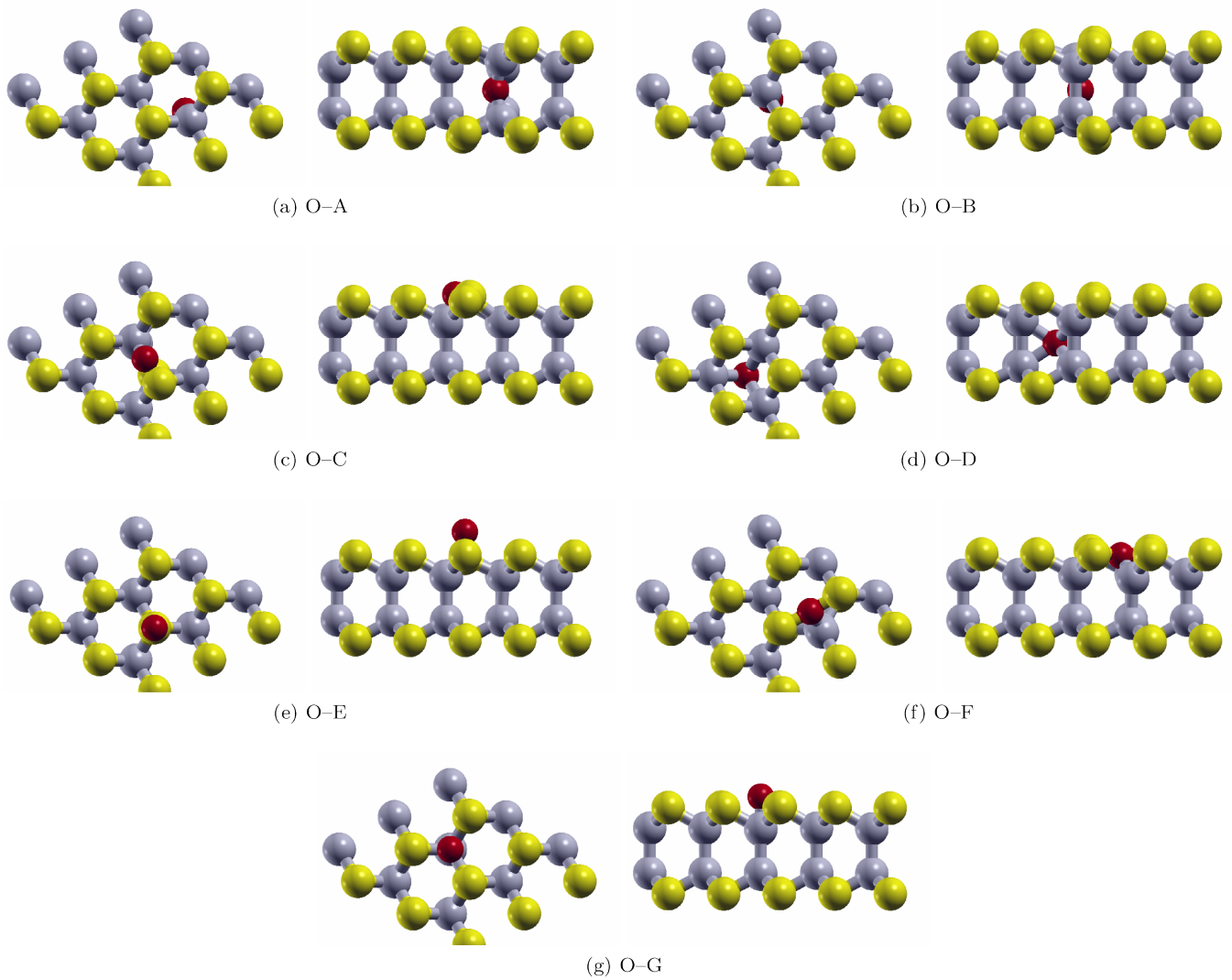


FIG. 6. (Color online) Top (0001) and side ($11\bar{2}0$) views of the stable single oxygen atom addition defects in monolayer InSe (Chemisorption), in increasing order of relative energy cost of formation. (a) O-A: interstitial oxygen defect between two indium atoms, with angled bonds like in water molecule, venturing out into the hexagonal interstitial cage. (b) O-B: interstitial oxygen in angled bond between two indium atoms, underneath (bridge) bond of indium-selenium. (c) O-C: oxygen in angled bond between indium and selenium. (d) O-D: interstitial oxygen at center of hexagonal cage. (e) O-E: oxygen above selenium. (f) O-F: three-coordinated oxygen between two selenium atoms, also bonded with indium atom. (g) O-G: oxygen above indium. The case of oxygen atom hovering above the center of the hexagonal interstitial cage is not stable.

- ¹⁸ A. Segura, K. Wünnstel, and A. Chevy, *Appl. Phys. A* **31**, 139 (1983).
- ¹⁹ J. Martinez-Pastor, A. Segura, C. Julien, and A. Chevy, *Phys. Rev. B* **46**, 4607 (1992).
- ²⁰ H. Chen, Y. Li, L. Huang, and J. Li, *RSC Adv.* **5**, 50883 (2015).
- ²¹ Z. Rak, S. D. Mahanti, K. C. Mandal, and N. C. Fernelius, *J. Phys.: Cond. Mat.* **21**, 015504 (2008).
- ²² Z. Rak, S. Mahanti, K. C. Mandal, and N. Fernelius, *J. Phys. Chem. Solids* **70**, 344 (2009).
- ²³ X. Li, C. Xia, X. Song, J. Du, and W. Xiong, *J. Mat. Sci.* **52**, 7207 (2017).
- ²⁴ H. Chen, Y. Li, L. Huang, and J. Li, *J. Phys. Chem. C* **119**, 29148 (2015).
- ²⁵ K. A. Kokh, Y. M. Andreev, V. A. Svetlichnyi, G. V. Lanskii, and A. E. Kokh, *Cryst. Res. Technol.* **46**, 327 (2011).
- ²⁶ C. Huang, Z. Wang, Y. Ni, H. Wu, and S. Chen, *RSC Adv.* **7**, 23486 (2017).
- ²⁷ Z. Rak, S. D. Mahanti, K. C. Mandal, and N. C. Fernelius, *Phys. Rev. B* **82**, 155203 (2010).
- ²⁸ I. Miyake, T. Tanpo, and C. Tatsuyama, *Jpn. J. Appl. Phys.* **23**, 172 (1984).
- ²⁹ N. Balakrishnan, Z. R. Kudrynskyi, E. F. Smith, M. W. Fay, O. Makarovskiy, Z. D. Kovalyuk, L. Eaves, P. H. Beton, and A. Patané, *2D Mat.* **4**, 025043 (2017).
- ³⁰ P. Hohenberg and W. Kohn, *Phys. Rev.* **136**, B864 (1964).
- ³¹ W. Kohn and L. J. Sham, *Phys. Rev.* **140**, A1133 (1965).
- ³² P. Giannozzi, S. Baroni, N. Bonini, M. Calandra, R. Car, C. Cavazzoni, D. Ceresoli, G. L. Chiarotti, M. Cococcioni,

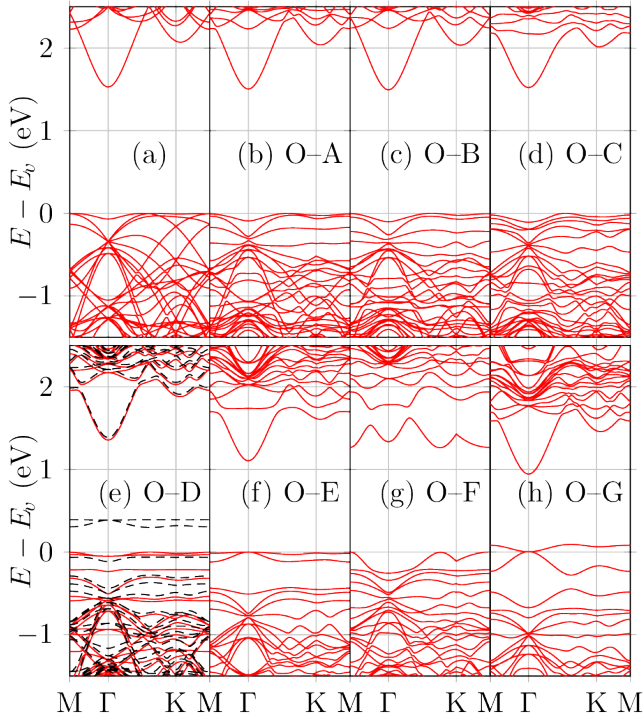


FIG. 7. (Color online) DFT band structure plots of various stable single oxygen atom defects in monolayer InSe (Chemisorption) in increasing order of relative energy cost of formation. (a) Pristine 3x3 supercell; (b)–(h) different configurations of oxygen defects. Refer to Fig. 6 for the respective defects. (e) is a magnetic spin calculation without spin-orbit coupling. Minority spin in dashes.

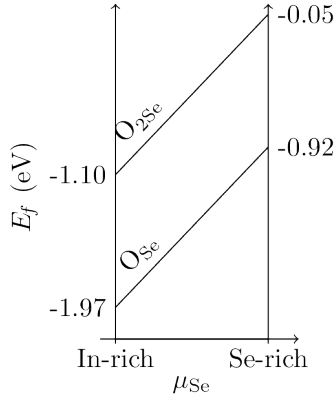


FIG. 8. Formation Energies E_f as a function of chemical potential μ_{Se} (arbitrary units) for oxygen substitution defects. $\Delta\mu_{\text{Se}} = 1.05$ eV. Refer to text for constraints and definitions.

I. Dabo, A. D. Corso, S. de Gironcoli, S. Fabris, G. Fratesi, R. Gebauer, U. Gerstmann, C. Gougoussis, A. Kokalj, M. Lazzeri, L. Martin-Samos, N. Marzari, F. Mauri, R. Mazzarello, S. Paolini, A. Pasquarello, L. Paulatto, C. Sbraccia, S. Scandolo, G. Sclauzero, A. P. Seitsonen, A. Smogunov, P. Umari, and R. M. Wentzcovitch, *J. Phys. C* **21**, 395502 (2009).

³³ Version 6.

³⁴ P. E. Blöchl, *Phys. Rev. B* **50**, 17953 (1994).

³⁵ G. Kresse and D. Joubert, *Phys. Rev. B* **59**, 1758 (1999).

³⁶ J. P. Perdew, K. Burke, and M. Ernzerhof, *Phys. Rev. Lett.* **77**, 3865 (1996).

³⁷ A. D. Corso, *Comput. Mat. Sci.* **95**, 337 (2014).

³⁸ Versions 0.3.1 and 1.0.0.

³⁹ H. J. Monkhorst and J. D. Pack, *Phys. Rev. B* **13**, 5188 (1976).

⁴⁰ A. Carvalho and A. H. C. Neto, *Phys. Rev. B* **89**, 081406 (2014).

⁴¹ L. Debbichi, O. Eriksson, and S. Lebegue, *J. Phys. Chem. Lett.* **6**, 3098 (2015), pMID: 26267208.

⁴² D. Olguín, A. Rubio-Ponce, and A. Cantarero, *Euro. Phys. J. B* **86**, 350 (2013).

⁴³ R. M. de la Cruz, R. Pareja, A. Segura, and A. Chevy, *J. Phys. C* **21**, 4403 (1988).

⁴⁴ P. Giannozzi, R. Car, and G. Scoles, *J. Chem. Phys.* **118**, 1003 (2003).

⁴⁵ C. Han, Z. Hu, A. Carvalho, N. Guo, J. Zhang, F. Hu, D. Xiang, J. Wu, B. Lei, L. Wang, C. Zhang, A. H. C. Neto, and W. Chen, *2D Mat.* **4**, 021007 (2017).

⁴⁶ P. K. Gogoi, Z. Hu, and Q. W. et al., sub. to *Phys. Rev. Lett.* (2017).

⁴⁷ L. Schimka, J. Harl, and G. Kresse, *J. Chem. Phys.* **134**, 024116 (2011).

⁴⁸ Y. Liu, P. Stradins, and S.-H. Wei, *Angewandte Chemie International Edition* **55**, 965 (2016).

⁴⁹ A. Ziletti, A. Carvalho, D. K. Campbell, D. F. Coker, and A. H. Castro Neto, *Phys. Rev. Lett.* **114**, 046801 (2015).